Argon Scattering off the Surface of Liquid Indium: Exit Angle and Energy Dependence

L. Tribe, Michelle Manning, Jason A. Morgan, M. D. Stephens, Warren R. Ronk, E. Treptow, Gilbert M. Nathanson,* and J. L. Skinner*

Department of Chemistry, University of Wisconsin, Madison, Wisconsin 53706

Received: August 8, 1997; In Final Form: October 13, 1997[⊗]

Energy- and angle-resolved intensities are reported for the scattering of argon atoms off the surface of liquid indium just above the melting temperature, for two different argon incident energies. The higher incident energy results show significant energy transfer from argon to liquid atoms, and the angular distribution of scattered argon atoms is relatively sharply peaked near the specular angle. The lower incident energy results show a small amount of energy transfer from liquid atoms to argon atoms, the energy distribution of the scattered argon atoms is nearly thermal, and the angular distribution is much less sharply peaked, although still not completely thermal. Molecular dynamics simulations of these experiments are performed, and most of the results are in reasonable agreement with experiment. Analysis of the simulation trajectories helps to provide a microscopic understanding of the experimental results.

1. Introduction

Many physical and chemical phenomena involve collisions and reactions at gas−liquid interfaces. These processes include desiccation, stratospheric ozone depletion via sulfuric acid areosols,[1,2] and the destruction of toxic compounds in molten metals.[3] A key step in many gas−liquid reactions is the initial energy transfer between gas and surface molecules, since this brings the gas species into longtime contact with the liquid.[4−6]

This paper describes a theoretical and experimental investigation of argon scattering off the surface of liquid indium. We focus on the energy and angular distributions of the scattered argon atoms, which also provide information about the structure and dynamics of the indium liquid−vapor interface. By studying this relatively simple system we hope to provide a microscopic picture of the ways in which gas atoms scatter from and transfer energy to the surface atoms of a liquid.

Previous theoretical and experimental studies of the structure of the liquid−vapor interface for metallic systems include self-consistent Monte Carlo simulations[7] and X-ray reflection and diffraction measurements.[8−14] Theoretical approaches to atom scattering from liquid metal surfaces include single-collision kinematic models[15] and classical scattering theory,[19] while molecular dynamics computer simulations have been carried out for atom scattering from other liquid surfaces.[20,21] The latter are particularly appealing because the many-body nature of the structure and dynamics of the interface and of the scattering process are explicitly taken into account.

Liquid indium is convenient to study experimentally because of its low melting point (430 K) and low vapor pressure ($<10^{-9}$ Torr). From a theoretical perspective indium is attractive because, even though the liquid state is metallic, the bulk radial distribution function has the form of simple atomic liquids,[22−27] indicating that perhaps one can describe the liquid and its interface using a model with simple pairwise additive potentials. Previous experimental studies of energy transfer between Ar and liquid In at fixed incident and exit angles[6] are complemented in the present paper with new results on the exit angle dependence of the scattered intensity. The experimental exit angle and energy distributions are compared with results from classical molecular dynamics computer simulations. Through an analysis of individual trajectories, the simulations reveal many of the different pathways for energy transfer between gas and liquid.

2. Experimental Methods and Results

The experimental data consist of time-of-flight (TOF) spectra and total flux in-plane angular distributions of argon atoms scattering from liquid indium. Nearly monoenergetic beams of Ar are directed at the center of a 1.9 cm diameter by 0.2 cm deep crucible filled with 0.5 mL of 99.999% indium inside an ultrahigh-vacuum chamber. The liquid temperature, T, is maintained at 436 ± 2 K, which is 6 K above the melting point of In.

The TOF spectra are graphs of number density $N(t)$ versus the arrival time t at a mass spectrometer located 28.8 cm from the surface. All TOF spectra are for in-plane scattering at fixed incident and final angles, θ_i and θ_f, of 55° with respect to the surface normal. Thus the TOF apparatus monitors scattering at the specular angle. The relative fluxes or intensities, $I(E_f)$, of argon atoms scattering from liquid indium are derived from the TOF spectra using the relation $I(E_f) = N(t)t^2$, where the recoil energy $E_f = (1/2)m_{Ar}(L/t)^2$ and $L = 28.8$ cm. $I(E_f)$ is proportional to the probability that an Ar atom will scatter from indium at a final energy E_f. The TOF spectra and data analysis are described in ref 6.

The total flux angular distributions, $I(\theta_f)$, are recorded by measuring the scattered flux as a function of θ_f from −30° to 80° within the scattering plane. The recoiling atoms pass through a 0.32 cm diameter aperture located 5.4 cm from the surface before traveling through a corrugated tube attached to the stationary mass spectrometer. The aperture rotates about the surface with an angular resolution of ±2°. A detailed report of the angular distributions of inert gases scattering from liquid In, Ga, and Bi will be presented in a forthcoming paper.[28]

The energy distributions of the scattered Ar atoms for two different incident energies, E_i, are shown in Figures 1 and 2.

[⊗] Abstract published in *Advance ACS Abstracts,* December 1, 1997.

S1089-5647(97)02596-0 CCC: $15.00
Published on Web 01/01/1998

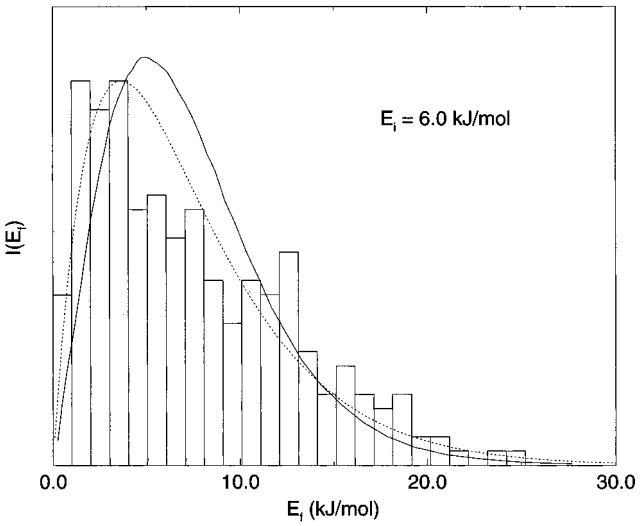

Figure 1. Scattered intensity, $I(E_f)$, as a function of final energy, E_f, for $\theta_i = \theta_f = 55°$ (specular scattering) and for $E_i = 6.0$ kJ/mol. The solid line is the experimental data, and the histogram is from the simulation. The dotted line is the (flux-averaged) thermal distribution given by eq 2.1.

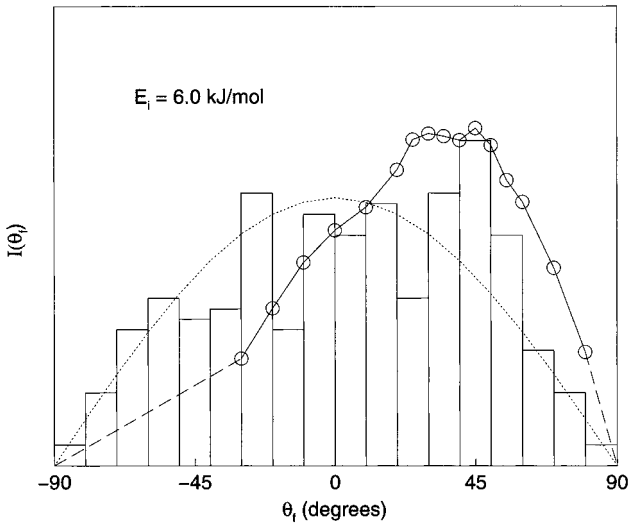

Figure 3. Scattered intensity as a function of in-plane scattering angle, integrated over all final energies, for $E_i = 6.0$ kJ/mol. The circles are the experimental points (which are connected by solid lines), and the histogram is from the simulation. The dotted line is the (flux-averaged) thermal distribution prediction, which is proportional to cos θ_f.

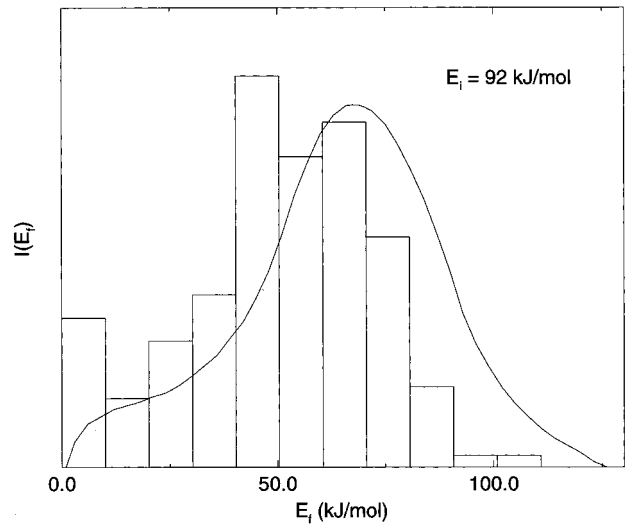

Figure 2. Same as Figure 1 but for $E_i = 92$ kJ/mol.

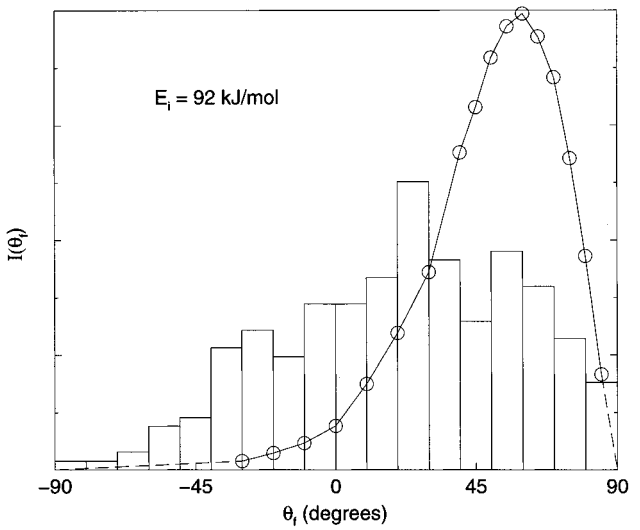

Figure 4. Same as Figure 3 but for $E_i = 6.4$ kJ/mol.

Figure 1 reveals that the most probable and average recoil energies for Ar atoms with $E_i = 6.0$ kJ/mol are 5.0 and 7.4 kJ/mol, respectively. Thus, at this low impact energy, the scattered atoms on average gain energy from the liquid. For comparison, a flux-weighted Boltzmann distribution, given by

$$I(E_f) = \frac{E_f}{(RT)^2} e^{-E_f/RT} \quad (1)$$

is also shown in Figure 1. The peak and average energies of this thermal distribution are 3.6 and 7.2 kJ/mol, respectively. Although the experimental and thermal distributions yield almost the same average energy, the experimental distribution peaks at higher E_f. For Ar atoms with $E_i = 92$ kJ/mol (Figure 2), the most probable final recoil energy is 65 kJ/mol and the average final energy is 60 kJ/mol, corresponding to an average energy transfer of 35%. The shoulder at low E_f overlaps only slightly with the thermal distribution, suggesting that it represents atoms undergoing extensive energy transfer but not complete thermalization.

The total flux angular distributions shown in Figures 3 and 4 indicate that argon atoms recoil primarily in the forward direction ($\theta_f > 0°$). The angular distribution for Ar atoms at $E_i = 6.0$ kJ/mol (Figure 3) peaks between 25° and 50°. The dotted line is a cosine distribution, which is expected for atoms exiting by thermal desorption.[29,30] The experimental angular distribution is narrower than cosine and peaks in the forward direction. The absence of symmetry about $\theta_f = 0°$ indicates that the departing argon atoms are not completely thermalized. For Ar at $E_i = 92$ kJ/mol (Figure 4), the angular distribution peaks narrowly around $\theta_f = 60°$. Only a small fraction of the atoms scatter in the backward direction ($\theta_f < 0°$). These high incident energy Ar atoms exhibit a narrower, more forward peaked angular distribution with less backscattering than the lower incident energy Ar atoms.

3. Theoretical Model and Simulation Method

As discussed in the Introduction, even though liquid indium is metallic, it can be described reasonably well by simple pairwise interactions.[22−27] In fact, we choose the simplest nontrivial two-body potential for the indium−indium interaction,

that of the Lennard-Jones potential:

$$\Phi(r) = 4\epsilon\left[\left(\frac{\sigma}{r}\right)^{12} - \left(\frac{\sigma}{r}\right)^{6}\right] \quad (2)$$

σ and ϵ are the "diameter" and well depth, respectively.

Our choices for the values of these parameters were determined by the following. Liquid indium has a very low vapor pressure, which makes it ideal for scattering experiments because one is confident that the incoming atoms are scattering off liquid-phase rather than gas-phase atoms. We would also like the simulated liquid to have a low vapor pressure, to accurately model the real situation, and to avoid simulated scattering events off gas-phase atoms. To this end we choose the coexisting liquid to have a temperature of $kT/\epsilon \equiv T^* = 0.73$, slightly above the triple temperature ($T^* = 0.69$) for the Lennard-Jones fluid.[31] At this temperature the corresponding density on the coexistence line is $\rho\sigma^3 \equiv \rho^* = 0.83$.[31] With these values of ρ^* and T^*, the temperature of the liquid in these experiments (436 K) and the experimental liquid density (7.03 g/cm^3)[32] can be used to determine σ and ϵ, leading to $\sigma = 282$ pm and $\epsilon/k = 597.3$ K. In fact we chose slightly different values, $\sigma = 281$ pm and $\epsilon/k = 606.8$ K, corresponding to a temperature ($T = 443$ K) and density (7.13 g/cm^3) only slightly different from the experimental values.

As one assessment of the appropriateness of this potential and these parameters for liquid indium, we calculate the radial distribution function for this Lennard-Jones liquid at $\rho^* = 0.83$ and $T^* = 0.73$ using the very accurate HMSA integral equation.[33,34] Defining r_{max} to be the value of r at the maximum in the first peak of $g(r)$, we find, for example, that $r_{max} = 304$ pm and that $g(r_{max}) = 2.98$. These values are in rough agreement with the experimental values for liquid indium of 314 pm and 2.66, respectively.[32]

We also assume that the indium−argon interaction is given by a Lennard-Jones potential. Taking the standard Lennard-Jones parameters for argon of $\sigma = 341$ pm and $\epsilon/k = 119.8$ K,[35] and using the standard combining rules for two-component Lennard-Jones systems,[35] we arrive at the following parameters for the argon−indium Lennard-Jones parameters: $\sigma_0 = 311$ pm and $\epsilon_0/k = 269.6$ K.

To perform a classical molecular dynamics simulation of argon scattering off the surface of liquid indium, we must first simulate liquid indium in equilibrium with its vapor. To do so, we begin by simulating neat liquid indium at a reduced temperature and density of $T^* = 0.85$ and $\rho^* = 0.85$. This simulation is carried out using the velocity-Verlet algorithm[36] with periodic boundary conditions. The initial configuration, of 864 atoms, is a face-centered cubic lattice, and the total momentum of the system is zero. The equations of motion are integrated and the velocities of the particles are rescaled periodically until the desired temperature is obtained. This equilibration phase of the simulation was run for about 10 000 time steps of 6.7 fs each.

Next, the length of one of the edges of the simulation cube is doubled, so that initially the box is composed of two cubes, one full of particles and the other empty. Periodic boundary conditions for the new box are now imposed. This initial configuration is then equilibrated for 2 000 time steps. During this second equilibration phase the temperature falls, as kinetic energy is converted to potential energy, reaching an equilibrated value of $T^* = 0.73$. At this new temperature and the new total density (half of the original density), the system is in the liquid−vapor coexistence regime. Therefore the simulation volume has coexisting liquid and vapor phases. The density profile along the z axis (the axis along which the cube was doubled) is shown in Figure 5. One sees well-defined liquid and vapor phases with an interface between them. We note that this profile does not show the oscillations that have been found theoretically and experimentally for other liquid metals.[11−13] Indeed, a profile obtained from Lennard-Jones pair potentials could never produce such oscillations. From our simulation one determines that the liquid and vapor densities are, respectively, $\rho^* = 0.82$ and 0.0031, in excellent agreement with the coexisting densities at the same temperature from the best available Lennard-Jones equation of state, which are 0.83 and 0.0031.[31] Defining the "vapor phase" to be the region with $z/\sigma > 7.5$ (in this region the density profile in Figure 5 is constant), the above value for the vapor density shows that, on the average, there is less than one indium atom in this region. Therefore, in the simulations to be described, scattering off vapor-phase indium atoms occurs only very infrequently.

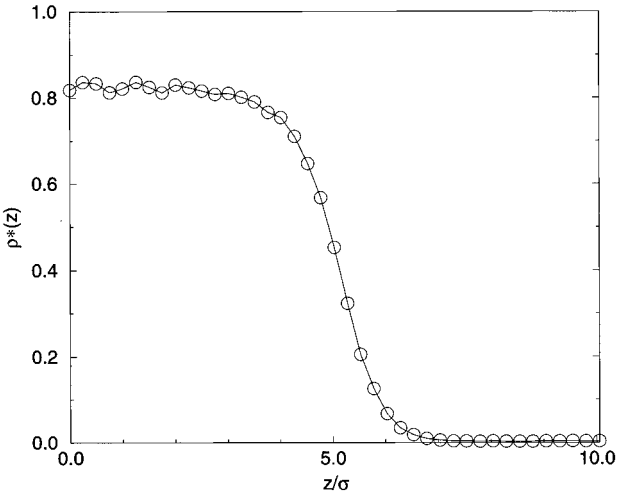

Figure 5. Density profile of the liquid−vapor interface.

From the simulated interface we can calculate the surface tension from[37]

$$\gamma = \frac{1}{2a^2}\left\langle \sum_{i>j}\left[\frac{(x_i - x_j)^2 + (y_i - y_j)^2 - 2(z_i - z_j)^2}{r_{ij}}\right]\Phi'(r_{ij})\right\rangle \quad (3)$$

where a^2 is the area of the face of the simulation cell parallel to the interface, x_i, y_i, z_i are the Cartesian coordinates of atom i, r_{ij} is the distance between atoms i and j, and $\Phi'(r)$ is the derivative of $\Phi(r)$ with respect to r. We obtain a value of 184 dyn/cm, which is smaller than the experimental value for indium, 556 dyn/cm,[32] by about a factor of 3. This disagreement indicates that our interface is probably rougher than the experimental interface. To put this in perspective we note that experimental values of the liquid−vapor surface tension vary over a very wide range (from 8.75 dyn/cm for N_2 to 2700 dyn/cm for Re).[38,39]

To simulate scattering events, we send in an argon atom with a velocity vector angled 55° with respect to the surface normal and with a well-defined kinetic energy. The entire system, liquid and vapor plus incoming particle, now obeys Newton's equations. The simulation is run while the particle moves toward the surface, interacts with it, and leaves the simulation volume again. When the particle leaves the simulation box, its energy is recorded, as well as its in-plane and out-of-plane scattering angles. This scenario is repeated many times, choosing random initial positions for the incoming particle and random configurations of the liquid−vapor system. Simulations were performed

for two different initial argon kinetic energies, 6.4 and 92 kJ/mol, to approximately match the experiments reported herein. In the former case the simulation was run with a time step of 6.7 fs for a maximum of 134 ps. In the latter case, a time step of 1.3 fs was taken, for a maximum time of 40 ps. The argon atoms left the surface before the maximum time in all but a few cases.

4. Simulation Results and Comparison to Experiment

We simulated 4000 scattering events for incoming argon atoms with 92 kJ/mol of kinetic energy and another 4000 events for argon atoms with 6.4 kJ/mol. Each scattered argon atom is characterized by its final energy and by its angular deflection. In this paper we will only be concerned with in-plane scattering. To compare with experiment, we consider the energy dependence of the intensity at a fixed exit angle of 55°, and also the in-plane angular dependence, integrated over all energies, of the scattered intensity. In the former case, if we make the solid angle of the "detector" too small, our statistics will be poor. Therefore, the theoretical detector by necessity is somewhat larger than in the experiment: it detects a cone of particles whose boundaries are 20° from the center line. For the angular dependence the statistics are much better (since one integrates over all energies), and we choose a cone whose boundaries are 5° from the center line.

The simulation results for the final energy dependence of the high-energy incident beam are shown in Figure 2. One sees that while the agreement with experiment is not quantitative, it is still quite good. The average energy of the simulated intensity is 50.3 kJ/mol, in reasonable agreement with the experimental result of 60 kJ/mol. Furthermore, the simulation, like the experiment, seems to have enhanced scattering at low energy (more about which will be discussed below). The simulated energy dependence of the low-energy beam is shown in Figure 1. In this case the agreement between simulation and experiment is again quite good. The average energy of the simulated intensity, 7.5 kJ/mol, is in excellent agreement with the experimental result of 7.4 kJ/mol. The simulation results are also in good agreement with the thermal distribution.

The simulation results for the angular dependence of the scattered intensity for the high-energy beam are shown in Figure 4. Here one sees that the agreement with experiment is not very good, and the simulated results are less sharply peaked and with significantly more backscattering than in the experiments. Thus it appears that the simulated surface is rougher than the experimental one, in accord with our conclusion from the surface tension calculation. The simulation results for the angular dependence of the low-energy beam are shown in Figure 3. Here one sees that agreement between simulation and experiment is much better. This presumably is because the scattered intensity is approaching a thermal distribution, in which case it does not matter as much whether the surface is rough or smooth.

The energy dependence of the scattered beam has not been measured experimentally for exit angles other than $\theta_f = 55°$. From the simulation, however, we do in principle have this information. To obtain good angular resolution we have used the "narrow" detector described above and have calculated the average scattered energy as a function of in-plane scattering angle. Our results for the two incident energies are shown in Figure 6. We see that for the low-energy beam the average energy is roughly independent of scattering angle, providing further evidence that in the simulation the scattered beam is close to being thermalized by the surface. For the high-energy beam the average energy falls more or less monotonically with the magnitude of the deflection angle ($180° - (\theta_f + 55°)$), in qualitative agreement with hard-sphere models of two-body scattering.[15] This may make some sense, since at these high energies the incoming particles interact strongly with the repulsive wall of the metal atom potentials, and (as we will see below) there are not too many "collisions" with metal atoms.

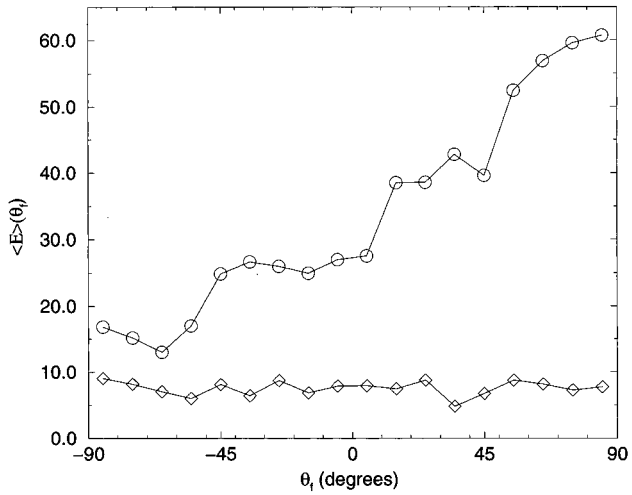

Figure 6. Average scattered energy as a function of in-plane scattering angle. The circles are from the simulation of the 92 kJ/mol beam, and the diamonds are from the simulation of the 6.4 kJ/mol beam.

One of the advantages of a microscopic simulation is that we can examine in detail individual trajectories of the argon atoms. In particular, we are interested in characterizing the number of "collisions" with metal atoms. To this end we have found it useful to output, throughout the scattering event, the z coordinate of the position of the argon particle, the kinetic energy of the argon particle, and the dot product of the argon's velocity unit vector at one time step with the velocity unit vector at the subsequent time step.

For a particular trajectory of a high-energy incident argon atom that scatters into the "narrow" detector at $\theta_f = 55°$, these quantities are shown in Figure 7. First considering the z coordinate, one sees that the argon atom approaches the surface with constant velocity and at about $t = 900$ fs turns around and proceeds out from the surface with a slower velocity. In fact the kinetic energy of the argon atom exemplifies a single collision with a metal atom: the kinetic energy first increases as the argon is accelerated by the attractive potential, then the kinetic energy decreases as the argon climbs the repulsive wall of a metal atom, after a hard-sphere-like "collision" the kinetic energy increases as the argon is accelerated by the attractive part of the potential, and finally the argon is decelerated as it leaves the attractive part of the potential.[16] This single collision picture is corroborated by the argon's velocity unit vector, which shows a single abrupt change at the moment of the collision.

We examined 16 such random trajectories for the high-energy beam, and surprisingly, we found that only 4 of the 16 could be characterized by a single collision. Eight of the 16 were best described by double collisions, while 4 of the 16 were best described by three collisions. A typical triple-collision scattering event is shown in Figure 8. Of these 16 events it is interesting to examine the correlation between number of collisions and final energy, which is shown in Figure 9. One sees that the "single-collision" atoms lost the most energy on the average and that the final energy of the "triple-collision" atoms varied widely. This figure shows, roughly, how single, double, and

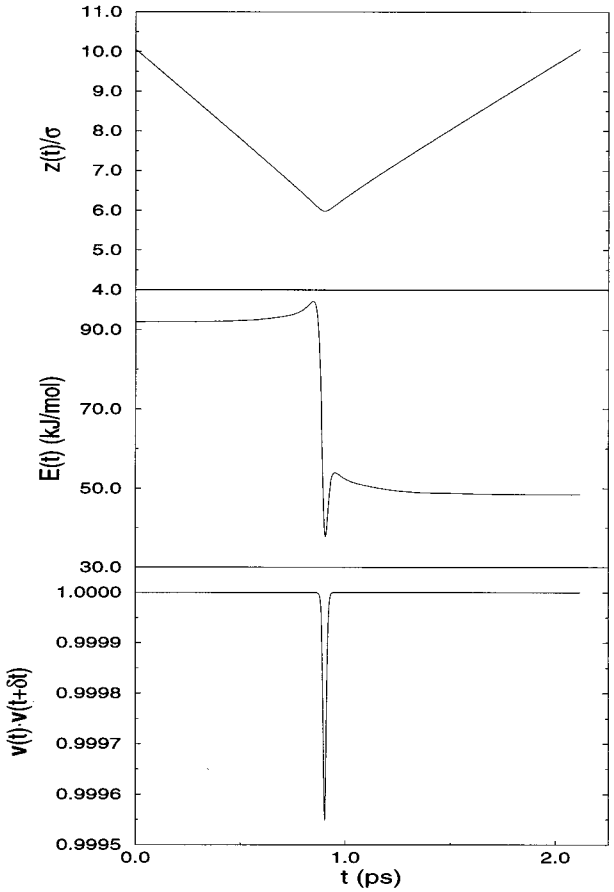

Figure 7. "Single-collision" trajectory of an argon atom incoming with 92 kJ/mol kinetic energy. The top panel shows the position (z coordinate) of the atom as a function of time, the second panel shows its kinetic energy, and the bottom panel shows the dot product of the atom's velocity unit vector at time t, $v(t)$, with its velocity unit vector at a time δt (a single time step) later.

triple collision scattering events contribute to the simulated histogram in Figure 2. In particular, a fixed exit energy cannot be associated with a specific number of collisions. For these 16 trajectories we have also determined the distance of closest approach to the liquid; the average distance of closest approach is $z/\sigma = 6.04$. This implies roughly that the incoming argon atoms interact with metal atoms whose centers are one diameter closer in, or about $z/\sigma \simeq 5$, which is about the middle of the interface (see Figure 5).

It is also interesting to examine specifically the events that lead to the low-energy bump in the simulated energy distribution in Figure 2. (Recall that this distribution was obtained for the "wide" detector.) We find that these trajectories mostly involve more than 10 collisions with metal atoms. Thus it is not surprising that this low-energy peak occurs for energies on the order of RT.

Finally we turn to the low-energy incident beam. In this case we examined 9 trajectories in detail, finding that one was a single-collision event, one involved a triple collision, one involved 9 collisions, and six involved 10 or more collisions. Thus it is not surprising that in this case the simulated energy and angular distributions are close to thermal. A typical trajectory involving multiple collisions is shown in Figure 10. The average distance of closest approach for these 9 trajectoires is $z/\sigma = 5.12$, showing that these low-energy argon atoms have penetrated much more deeply into the interface.

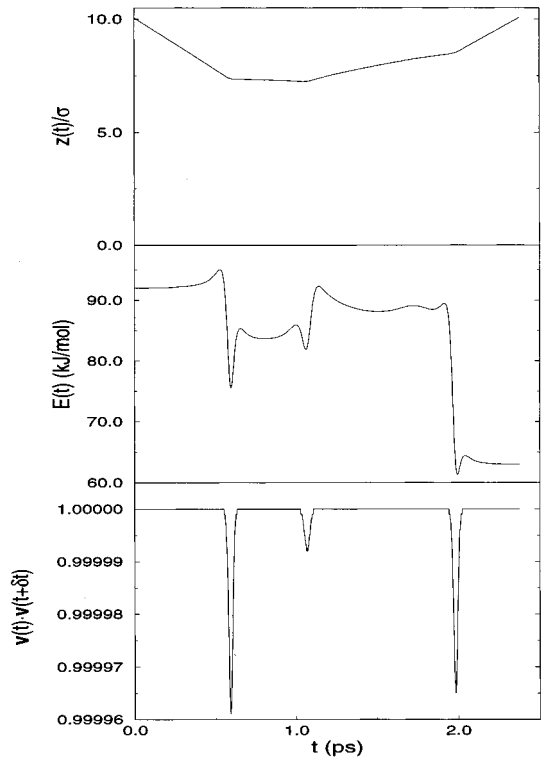

Figure 8. Same as Figure 7 but for a "triple-collision" trajectory.

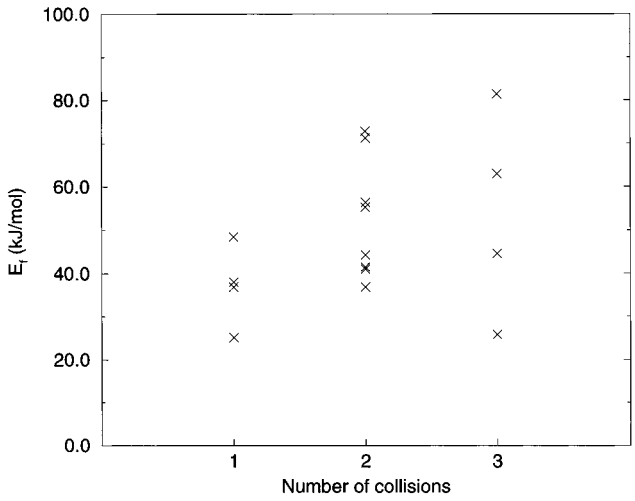

Figure 9. Final energy versus number of collisions for 16 randomly chosen trajectories of 92 kJ/mol atoms scattering at the specular angle.

5. Conclusions

Atom scattering off liquid surfaces provides important information about gas−liquid energy-transfer processes. It is also a powerful method for exploring the structure and dynamics of the liquid−vapor interface. The experiments are especially revealing when coupled with atomic-level theory. Our molecular dynamics calculations are in qualitative, and sometimes quantitative, agreement with experiment. As such, they support the idea that most scattering events involve many metal atoms and multiple collisions.

The most glaring disagreement between simulation and experiment comes from the angular dependence of the scattering intensity for the high-energy beam of argon atoms. We have expressed our belief that the simulated surface is rougher than the experimental one, thus leading to this discrepancy. This indicates that a more accurate and sophisticated description of

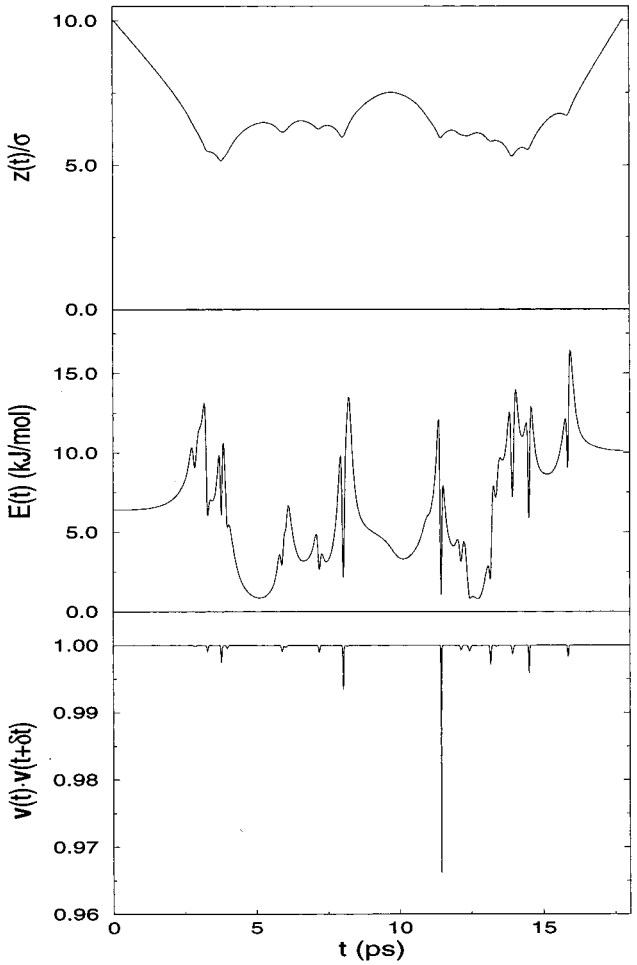

Figure 10. Same as Figures 7 and 8, but for an atom whose initial energy is 6.4 kJ/mol.

the liquid metal is needed. A particularly attractive many-body approach is the embedded atom method.[40] Work in this direction is in progress.[41]

Acknowledgment. J.L.S. and G.M.N. are thankful for support from the National Science Foundation through Grants CHE-95626815 and CHE-9417909, respectively.

References and Notes

(1) Jayne, J. T.; Worsnop, D. R.; Kolb, C. E.; Swartz, E.; Davidovits, P. *J. Phys. Chem.* **1996**, *100*, 8015.
(2) Lovejoy, E. L.; Hanson, D. R. J. *J. Phys. Chem.* **1996**, *100*, 6397.
(3) Nagel, C. J.; Chanenchuk, C. A.; Wong, E. W.; Bach, R. D. *Env. Sci. Technol.* **1996**, *30*, 2155.
(4) Klassen, J. K.; Nathanson, G. M. *Science* **1996**, *273*, 333.
(5) Fiehrer, K. M.; Nathanson, G. M. *J. Am. Chem. Soc.* **1997**, *119*, 251.
(6) Ronk, W. R.; Kowalski, D. V.; Manning, M.; Nathanson, G. M. *J. Chem. Phys.* **1996**, *104*, 4842.
(7) D′Evelyn, M. P.; Rice, S. A. *J. Chem. Phys.* **1983**, *78*, 5081.
(8) Bosio, L.; Oumezine, M. *J. Chem. Phys.* **1984**, *80*, 959.
(9) Flom, E. B.; Cai, Z.; Acero, A.; Lin, B.; Maskil, N.; Liu, L.; Rice, S. A. *J. Chem. Phys.* **1992**, *96*, 4743.
(10) Flom, E. B.; Li, M.; Acero, A.; Maskil, N.; Rice, S. A. *Science* **1993**, *260*, 332.
(11) Rice, S. A. *J. Non-Cryst. Solids* **1996**, *205*−*207*, 755.
(12) Magnussen, O. M.; Ocko, B. M.; Regan, M. J.; Penanen, K.; Pershan, P. S.; Deutsch, M. *Phys. Rev. Lett.* **1995**, *74*, 4444.
(13) Regan, M. J.; Kawamoto, E. H.; Lee, S.; Pershan, P. S.; Maskil, N.; Deutsch, M.; Magnussen, O. M.; Ocko, B. M.; Berman, L. E. *Phys. Rev. Lett.* **1995**, *75*, 2498.
(14) Pershan, P. S. *Physica A* **1996**, *231*, 111.
(15) See ref 6, whose arguments are based on refs 16−18.
(16) Grimmelmann, E. K.; Tully, J. C.; Cardillo, M. J. *J. Chem. Phys.* **1980**, *72*, 1039.
(17) Tully, J. C. *J. Chem. Phys.* **1990**, *92*, 680.
(18) Harris, J. *Dynamics of Gas*−*Surface Interactions*; Rettner, C. T., Ashfold, M. N. R., Eds.; Royal Society of Chemistry: Cambridge, 1991.
(19) Muis, A.; Manson, J. R. *J. Chem. Phys.* **1997**, *107*, 1655.
(20) Lipkin, N.; Gerber, R. B.; Moiseyev, N.; Nathanson, G. M. *J. Chem. Phys.* **1994**, *100*, 8408.
(21) Benjamin, I.; Wilson, M.; Pohorille, A. *J. Chem. Phys.* **1994**, *100*, 6500.
(22) March, N. H. *Liquid Metals: Concepts and Theory;* Cambridge: London, 1990.
(23) Ocken, H.; Wagner, C. N. J. *Phys. Rev.* **1966**, *149*, 122.
(24) Orton, B. R.; Smith, S. P. *Philos. Magn.* **1966**, *14*, 873.
(25) Waseda, Y.; Suzuki, K. *Phys. Status Solidi B* **1972**, *49*, 339.
(26) Harris, M. L.; Collier, R. L.; Gruebel, R. W.; Callaway, T. O. *Phys. Lett.* **1978**, *65A*, 244.
(27) Ruppersberg, H.; Winterberg, K. H. *Phys. Lett.* **1971**, *34A*, 11.
(28) Manning, M.; Morgan, J. A.; Nathanson, G. M. Manuscript in preparation.
(29) Comsa, G.; David, R. *Surf. Sci. Rep.* **1985**, *5*, 145.
(30) Rettner, C. T.; Schweizer, E.; Mullins, C. B. *J. Chem. Phys.* **1989**, *90*, 3800.
(31) Johnson, J. K.; Zollweg, J. A.; Gubbins, K. E. *Mol. Phys.* **1993**, *78*, 591.
(32) Iida, T.; Guthrie, R. I. L. *The Physical Properties of Liquid Metals;* Clarendon: Oxford, 1988.
(33) Zerah, G.; Hansen, J.-P. *J. Chem. Phys.* **1986**, *84*, 2336.
(34) Egorov, S. A.; Stephens, M. D.; Yethiraj, A.; Skinner, J. L. *Mol. Phys.* **1996**, *88*, 477.
(35) Allen, M. P.; Tildesley, D. J. *Computer Simulations of Liquids;* Clarendon: Oxford, 1987.
(36) Swope, W. C.; Andersen, H. C.; Berens, P. H.; Wilson, K. R. *J. Chem. Phys.* **1982**, *76*, 637.
(37) Lee, J. K.; Barker, J. A.; Pound, G. M. *J. Chem. Phys.* **1074**, *60*, 1976.
(38) Evans, R. *J. Phys.* **1980**, *41 (C8)*, 775.
(39) Jasper, J. J. *J. Phys. Chem. Ref. Data* **1972**, *1*, 841.
(40) Daw, M. S.; Foiles, S. M.; Baskes, M. I. *Mater. Sci. Rep.* **1993**, *9*, 251.
(41) Chase, D.; Manning, M.; Morgan, J. A.; Nathanson, G. M.; Gerber, B. Manuscript in preparation.